Interfacial electrostatics guiding the crystallization of $CaCO_3$ underneath monolayers of calixarenes and resorcarenes†

Dirk Volkmer,*[a] Marc Fricke,[a] Ceno Agena[b] and Jochen Mattay[b]

[a]*Faculty of Chemistry (AC1), University of Bielefeld, P.O. Box 100 131, D-33501 Bielefeld, Germany. E-mail: dirk.volkmer@uni-bielefeld.de*
[b]*Faculty of Chemistry (OC1), University of Bielefeld, P.O. Box 100 131, D-33501 Bielefeld, Germany.*

The amphiphilic octaacids *rccc*-4,6,10,12,16,18,22,24-octakis-*O*-(carboxymethyl)-2,8,14,20-tetra(*n*-undecyl)resorc[4]arene (**1**) and 5,11,17,23,29,35,41,47-octakis(1,1,3,3-tetramethylbutyl)-49,50,51,52,53,54,55,56-octa(carboxymethoxy)calix[8]arene (**2**) form stable monolayers at the air–water interface which induce growth of $CaCO_3$ crystals at the monolayer–solution interface. Uniformly (012) oriented rhombohedral calcite single crystals grow underneath a monolayer of **2**, whereas crystallization under a monolayer of **1** preferentially leads to formation of acicular aggregates of aragonite crystals. While polymorph selection and orientations of the $CaCO_3$ crystals critically depend on the average charge density of the monolayer, the molecular shape and the particular Ca coordination behaviour of the amphiphiles that form the monolayer are of minor importance. $CaCO_3$ crystal growth underneath monolayers of macrocyclic amphiphiles is briefly reviewed and the present experimental observations are compared to previous related investigations on ''template-induced'' biomimetic mineralization.

Introduction

Crystallization of inorganic solids at self-organized surfaces is an important process in biomineralization[1] and crystal engineering.[2] Nucleation and growth steps taking place at the interface are often specific and result in a particular crystal polymorph or morphology.[3] However, the natural processes that control mineral formation are, as yet, poorly understood. Artificial matrices such as Langmuir monolayers,[4] self-assembled monolayers (SAMs),[5] and polymers[6] have been employed in order to gain insights into the putative mechanisms of template-directed mineralization. Physical parameters such as interfacial electrostatics[2,4,7] hydrogen bonding[3,5] and interfacial molecular recognition events including geometrical lattice matching[2,3] and stereochemical complementarity[8] are considered crucial factors in this context.

Calcium carbonate is the most abundant crystalline biomineral. Three stable $CaCO_3$ polymorphs—calcite, aragonite and vaterite—exist, all of which occur in calcified tissues. In order to mimic structural aspects of the interactions between acidic proteins and biogenic $CaCO_3$ in calcified tissues (*e.g.* mollusk shells) we employ Langmuir monolayers of macrocyclic oligoacids as biologically inspired supramolecular templates for crystal growth.

In previous studies we have reported on the growth of uniformly (012) oriented calcite single crystals underneath structurally diverse monolayers of tetracarboxy-calix[4]arenes[9] and tetracarboxy-resorc[4]arenes.[10] We have suggested that non-specific electrostatic effects such as charge density or mean dipole moment of the monolayer molecules determine the orientation of crystals. In order to further support this hypothesis we present here investigations on the crystallization of $CaCO_3$ underneath monolayers of two macrocyclic octacarboxylic acids (Scheme 1)

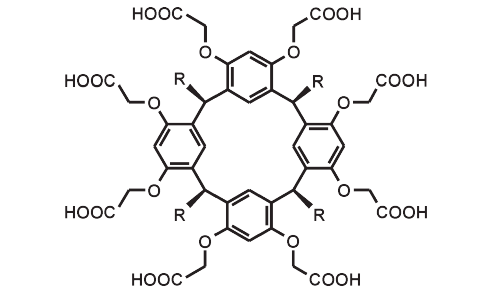

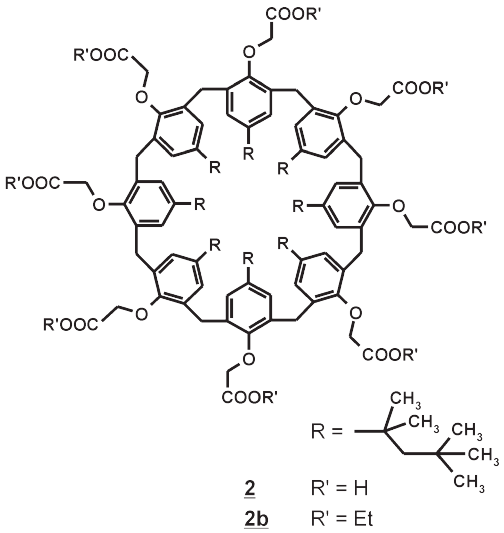

Scheme 1 Structural formulae of *rccc*-4,6,10,12,16,18,22,24-octakis-*O*-(carboxymethyl)-2,8,14,20-tetra(*n*-undecyl)resorc[4]arene (**1**) and 5,11,17,23,29,35,41,47-octakis(1,1,3,3-tetramethylbutyl)-49,50,51,52,53,54,55,56-octa(carboxymethoxy)calix[8]arene (**2**). (Compound **2b** is the ethyl ester derivative of **2**).

† Electronic supplementary information (ESI) available: representative optical and scanning electron micrographs of $CaCO_3$ crystals grown underneath a monolayer of **1** at low surface pressure; additional crystallographic data including numbering schemes, tables and refinement details. See http://www.rsc.org/suppdata/jm/b4/b403132f/

with different surface charge densities, namely *rccc*-4,6,10,12,16,18,22,24-octakis-*O*-(carboxymethyl)-2,8,14,20-tetra(*n*-undecyl)resorc[4]arene (**1**) and 5,11,17,23,29,35,41,47-octakis(1,1,3,3-tetramethylbutyl)-49,50,51,52,53,54,55,56-octa(carboxymethoxy)calix[8]arene (**2**). We describe an improved synthesis and the crystal structures of **1** and **2b** [5,11,17,23,29,35,41,47-octakis(1,1,3,3-tetramethylbutyl)-49,50,51,52,53,54,55,56-octa(ethoxycarbonylmethoxy)calix[8]arene, the ethyl ester of **2**. The dynamic macroscopic monolayer structure of **2** is characterized by means of Brewster angle microscopy (BAM). The growth of $CaCO_3$ crystals underneath monolayers of **1** and **2** is monitored *in situ* by (polarization) optical microscopy. Analysis of $CaCO_3$ growth morphologies is based on scanning electron microscopy and X-ray diffraction experiments. Using UV excitation, the luminescence of Mn^{2+}-doped $CaCO_3$ crystals is employed as spectroscopic probe in order to distinguish between different $CaCO_3$ polymorphs in complex crystal aggregates.

Results and discussion

X-Ray crystallographic investigations

Continuing our efforts on analysing typical solid state packing motifs of amphiphilic calixarene derivatives we here present X-ray crystallographic data of *rccc*-4,6,10,12,16,18,22,24-octakis-*O*-(carboxymethyl)-2,8,14,20-tetra(*n*-undecyl)resorc[4]arene (**1**) and 5,11,17,23,29,35,41,47-octakis(1,1,3,3-tetramethylbutyl)-49,50,51,52,53,54,55,56-octa(ethoxycarbonylmethoxy)calix[8]-arene (**2b**). We have previously shown that the average area per calixarene molecule in a Langmuir monolayer often is in good agreement with the corresponding value gleaned from its solid state structure provided that the amphiphilic compound forms a layered structure and the overall volume contribution of intercalated solvent molecules is negligible. Numerical differences between these two surface area values, on the other hand, are indicative of unusual packing arrangements of the amphiphiles at the air–water interface. Since large macrocyclic compounds such as resorcarenes and calixarenes can assume a variety of energetically equivalent conformations, the X-ray structures give us a glimpse of what their molecular shapes might look like and how these molecules could interact with their nearest neighbours in a monolayer.

Crystal structure of 1. X-Ray crystallographic investigations on single crystals of *rccc*-4,6,10,12,16,18,22,24-octakis-*O*-(carboxymethyl)-2,8,14,20-tetra(*n*-undecyl)resorc[4]arene (**1**) represent the second example of a *rccc*-resorcarene which contains *n*-undecyl and carboxylic acid residues. The crystal data of **1** may best be compared with those of *rccc*-5,11,17,23-tetracarboxy-4,6,10,12,16,18,22,24-octa-*O*-methyl-2,8,14,20-tetra(*n*-undecyl)resorc[4]arene (**3**) which we have reported previously.[10] Although the numbers and the substitution patterns of carboxylic acid groups are different, these two derivatives share common features in their molecular shapes and the packing in the crystal lattices.

Single crystals of **1** were obtained by crystallization at 90 °C from an acetic acid/H_2O solvent mixture (95/5 vol%). The conformational parameters which determine the resorcarene's molecular geometry are defined in Fig. 1.

The X-ray structure analysis shows that compound **1** adopts a boat conformation which is described by the folding angles $\varphi_{1,2}$ between least squares planes running through atomic positions of opposite benzene rings. In the present crystal structure of **1** φ_1 is 155.3°, while φ_2 amounts to 3.0°; the center-to-center spacing d between opposite benzene rings is 5.15 Å. For comparison: the corresponding values[11] from crystal data of **3** are: $\varphi_1 = 168.3°$, $\varphi_2 = 5.2°$, and $d = 4.93$ Å. The high similarity of the conformational parameters of compounds **1** and **3** suggests that the observed boat conformation primarily results from *intra*molecular bonding constrains of

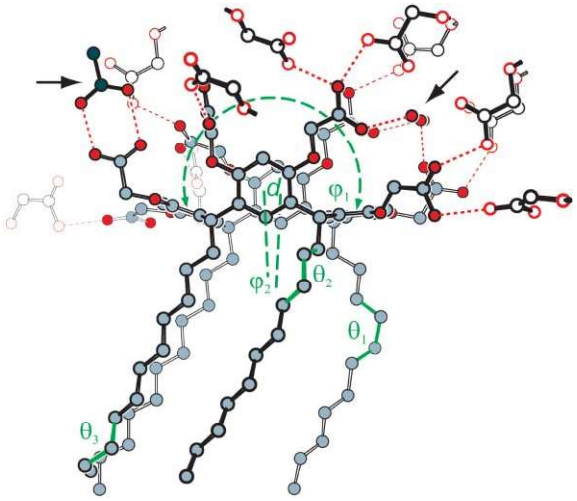

Fig. 1 Ball-and-stick model of the intermolecular hydrogen bonding scheme in the crystal lattice of **1**. Atoms belonging to neighbouring resorcarene molecules are displayed as open circles. Black arrows mark occluded acetic acid and water molecules. (Hydrogen atoms are omitted for clarity.) Definition of geometrical parameters used to describe the molecular structure of resorcarene moieties in the crystal structures of **1**. $\varphi_{1,2}$: folding angles between least squares planes running through atomic positions of opposite benzene rings; d: center-to-center spacing of opposite benzene rings; θ: torsion angle describing *gauche* "defects" occurring at selected atomic positions of the undecyl chains.

the macrocyclic ring system and is not due to specific *inter*molecular interactions between opposite resorcarene moieties in the crystal lattice. This statement gleans further support from the analysis of the hydrogen bonding scheme of carboxylic acid residues found in the crystal structure of **1**. Fig. 1 shows the hydrogen bonding scheme of compound **1** that makes hydrogen bonding contacts to six different nearest neighbours (of which only O–CH_2–COOH fragments are shown). The irregular arrangement of the pendent O–CH_2–COOH groups leads to deviation from ideal C_{2v}-symmety of the boat conformer. Hydrogen bonding occurs intra- as well as inter-molecularly. Based on O···O distance calculations a vast variety of equally strong hydrogen bonds are definable and thus an unequivocal assignment of the most likely positions of acidic protons is impossible. Beside the hydrogen bonding network between resorcarene moieties, some water and acetic acid molecules are found at structurally well-defined positions (black arrow markers in Fig. 1), both leading to a further reduction of the resorcarene's molecular symmetry. Of four undecyl chains only one adopts an energetically favourable all-*trans* conformation (the largest deviation from the ideal torsion angle, $\theta \sim 180°$, being 11.3°), the other ones display a single *gauche* "defect" (av. $\theta \sim 67.7°$) occurring at different atomic positions of the undecyl chains.

The irregular shape of the resorcarene molecules in the crystal lattice leads us to conclude that the supramolecular arrangement is primarily dictated by close-packing principles and not by directional forces between H-bonding donors/acceptors. Compound **1** thus forms a lamellar structure where the hydrophilic constituents (carboxylic acid residues) and the hydrophobic residues (undecyl chains) segregate into different layers. The stacking of layers occurs in *c*-direction of the crystal lattice (Fig. 2). Owing to the fact that each polar headgroup has hydrogen bonding contacts to six different resorcarene neighbours, the lamellae consist of two-dimensional bilayers which extend infinitely in the *ab*-plane of the crystal lattice (Fig. 2 shows an excerpt of a bilayer structure motif highlighted in green). The average surface area occupied by a single resorcarene molecule **1** in the *ab*-plane amounts to 1.71 nm^2 which corresponds to an average of 4.68 CO_2^- per nm^2. (Table 1 contains a comparative list of experimental monolayer

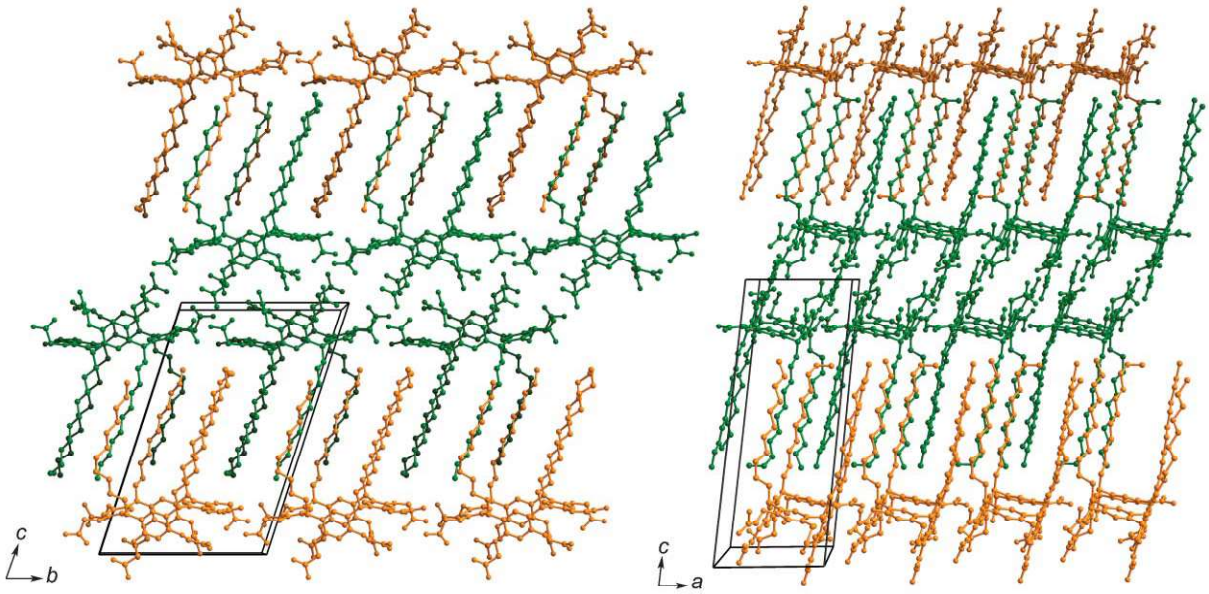

Fig. 2 Packing diagrams showing the interdigitation of bilayers of **1** in the crystal lattice. Resorcarene molecules belonging to the same "inverted" bilayer are represented with identical colors (hydrogen atoms are omitted for clarity).

Table 1 Correlation between area per molecule of amphiphiles used as crystallization templates and the $CaCO_3$ growth morphologies they induce

Compound	Area per molecule/nm^2			$COO^{\ominus}$/nm^2	Polymorph (pref. orientation if any)	Ref.
	Monolayer data	Crystal data	At which $CaCO_3$ crystals were grown			
1	1.65–1.70[a]	1.71				
	1.80–1.85[b]	n.d.	1.60–1.70	4.71–5.00	Aragonite, vaterite	This work
2	2.70–2.75[a]	n.d.				
	2.75–2.80[b]	n.d.	3.30–3.50	2.29–2.44	Calcite (012)	This work
			2.60–2.70	2.96–3.08	Calcite, vaterite	
2b	3.35–3.45[a]	3.23	n.d.	n.d.	n.d.	This work
3	1.75–1.80[b]	1.83	2.00–2.10	1.90–2.00	Calcite (012)	10
4	1.70–1.75[b]	1.70	1.75–1.80	2.22–2.29	Calcite (012)	9*a*
5	1.30–1.40[b]	1.70	1.70–1.80	2.35–2.42	Calcite (012)	9*b*
		1.33	1.25–1.35	3.01	Inhibition	
6	n.p.	0.43	π = 10 mN/m	4.65	Aragonite, vaterite	27
7	0.50[a]	n.d.	0.43–0.50	2.00–2.33	Calcite (012)	4*b*
8					Calcite (012)	6*a*
9	0.23–0.24[b]	n.d.	0.22–0.23	4.35–4.44	Calcite ($1\bar{1}0$), vaterite	20

[a] H_2O: doubly de-ionized water, resistance 18.2 MΩ cm. [b] $Ca(HCO_3)_2$: aqueous subphase containing $CaCl_2$/$NaHCO_3$, c = 9/18 mM. [c] n.d. = not determined; n.p. = not published. [d] Compound index (systematic names for amphiphiles not characterized in this work): **1**: $C_{88}H_{128}O_{24}$; **2**: $C_{136}H_{192}O_{24}$; **2b**; $C_{152}H_{224}O_{24}$; **3**: $C_{84}H_{128}O_{16}$, *rccc*-5,11,17,23-tetracarboxy-4,6,10,12,16,18,22,24-octa-*O*-methyl-2,8,14,20-tetra(*n*-undecyl)-resorc[4]arene; **4**: $C_{68}H_{96}O_{12}$, 5,11,17,23-tetrakis(1,1,3,3-tetramethylbutyl)-25,26,27,28-tetra(carboxymethoxy)calix[4]arene; **5**: $C_{52}H_{64}O_{12}$, 5,11,17,23-tetra-*tert*-butyl-25,26,27,28-tetrakis(carboxymethoxy)calix[4]arene; **6**: $C_{24}H_{38}O_5$, 5-hexadecyloxyisophthalic acid; **7**: N,N′-dioctadecyl-triazine-2,4,6-triamine and a cyanuric acid derivative; **8**: polymeric 10,12-pentacosadiynoic acid; **9**: $C_{18}H_{36}O_2$, stearic acid.

data for different amphiphiles). Fig. 3 shows a space filling model of the supramolecular packing arrangement of **1** in the crystal lattice. For clarity neighbouring resorcarene molecules

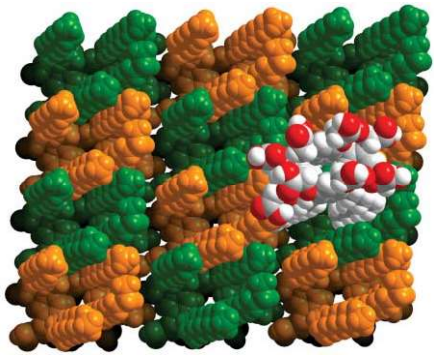

Fig. 3 Space-filling model of the supramolecular packing arrangement of **1** in the crystal lattice.

are distinguished by different colours (orange *vs*. green). Since the undecyl chains of an isolated bilayer are not bulky enough to fill the space completely (Fig. 3), interdigitation of successive bilayers occurs. The presence of *gauche* "defects" in the conformation of the undecyl chains may represent a further adaptation of the molecules to avoid empty spaces.

Crystal structure of 2b. All attempts to obtain single crystals of calix[8]arene octaacid **2** suitable for X-ray crystal structure investigations so far have failed. However, crystals of the corresponding ethylester derivative were readily available. Single crystals of 5,11,17,23,29,35,41,47-octakis(1,1,3,3-tetramethylbutyl)-49,50,51,52,53,54,55,56-octa(ethoxycarbonylmethoxy)-calix[8]arene ($C_{152}H_{224}O_{24}\cdot C_2H_5OH\cdot H_2O$, **2b**) were obtained by recrystallization from an ethanol solution containing 5% water. The X-ray structure analysis shows that the calix[8]-arene molecules adapt a highly symmetrical *flattened cone* conformation (Fig. 4a). Due to crystal packing effects the exact atom positions of the calixarene moiety differ from idealized C_4

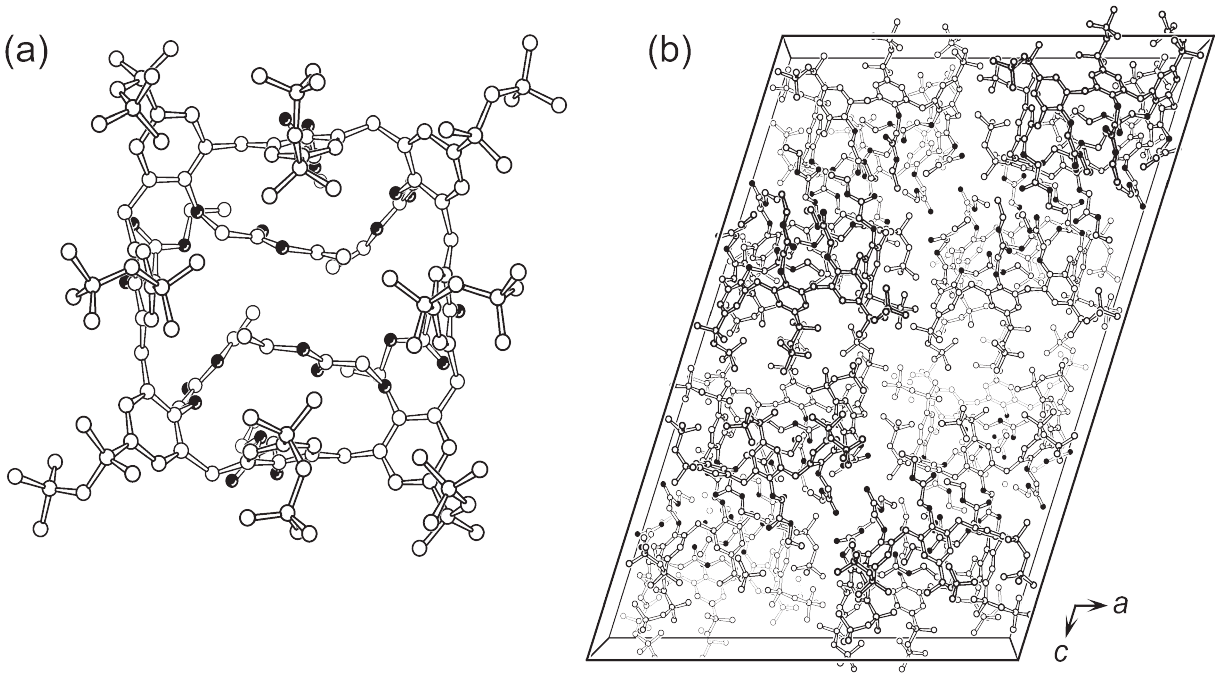

Fig. 4 (a) Ball-and-stick model of the molecular structure of **2b** (C and O atoms represented by open and black circles, respectively. Hydrogen atoms are omitted for clarity). (b) Ball-and-stick model of the supramolecular packing arrangement of **2b** in the crystal lattice (occluded solvent molecules and hydrogen atoms are omitted for clarity).

point symmetry. The ethoxycarbonylmethoxy substituents become irregularly placed such that two of them point inside the huge calix[8]arene cavity, while the neighbouring residues "hang down" from the lower rim which is defined by the circle of phenolic oxygen atoms. As a consequence, no further molecular guests are located within the internal cavities of **2b**, in contrast to host–guest inclusion phenomena frequently observed in conjunction with structurally similar calix[8]arene hosts.[12]

The conformation of the macrocyclic ring system can be defined by a few geometric parameters which are defined in Scheme 2. The midpoints R1–R8 of the benzene rings were calculated and individual distances from their common geometric centre Z are displayed in Table 2. Roughly speaking, the benzene rings show two regularly alternating tilt angles (av. values: 137° and 74°), and the distances Z–R*n* assume two different av. values (7.0 Å and 5.5 Å). For comparison: the corresponding geometric parameters of the C_2-symmetric compound 5,11,17,23,29,35,41,47-octakis(1,1,3,3-tetramethylbutyl)-49,50,51,52,53,54,55,56-octakis(2-methoxyethoxy)calix[8]arene[13]—which assumes a *chair* conformation—are 42°, 133°, 68°, 115°, and 7.3 Å, 6.2 Å, 5.0 Å, 6.7 Å, respectively. In both calix[8]arene derivatives the sterically demanding hydrophobic 1,1,3,3-tetramethylbutyl substituents at the upper rim are closely packed.

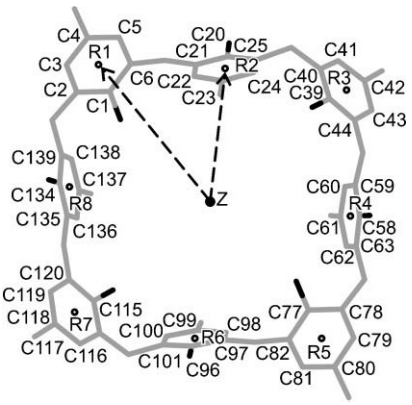

Scheme 2 Definition of geometrical parameters used to describe the molecular structure of the macrocyclic calix[8]arene moiety in the crystal structures of **2b**. R*n* denotes the midpoint of the *n*th benzene ring, Z is the geometric centre of R1–R8.

Compound **2b** forms a lamellar structure where the more hydrophilic constituents (ethoxycarbonylmethoxy substituents, crystal ethanol solvate) and the hydrophobic residues segregate into different layers. The bilayers run parallel to the crystallographic *ab*-plane and layer stacking follows the *c*-direction (Fig. 4b). Within the layer, calixarene molecules are close packed with their pseudo C_4 symmetry axis being tilted by 28° against the *ab*-plane normal. The average surface area occupied by a single calix[8]arene molecule in the *ab*-plane amounts to 3.23 nm^2.[14]

Monolayer studies

Crystallographic investigations on the solid state structures of **1** and **2b** are complemented by monolayer studies of **1** and **2**. Langmuir monolayers were formed on an aqueous subphase by spreading compound **1** from trichloromethane/tetrahydrofuran (4 : 1) and **2** from trichloromethane/methanol (9 : 1) solution using a Langmuir trough. The surface pressure–area (π–A) isotherms provide information on monolayer stability and phase behaviour. Fig. 5 shows the π–A isotherms of compound **1** and **2** monolayers after having been spread on pure water or

Table 2 Distances between the midpoints of benzene rings (R1–R8) of **2b** and their calculated geometric centre Z (left). Angles between l.s. planes through R1–R8 and l.s. planes through individual benzene rings (right)

Distance/Å		Angle/°	
Z···R1:	7.01	R1–R8/C1–C6:	146.9
Z···R2:	5.33	R1–R8/C20–C25:	73.4
Z···R3:	6.98	R1–R8/C39–C44:	125.2
Z···R4:	5.58	R1–R8/C58–C63:	74.1
Z···R5:	7.01	R1–R8/C77–C82:	147.4
Z···R6:	5.45	R1–R8/C96–C101:	74.2
Z···R7:	6.92	R1–R8/C115–C120:	127.9
Z···R8:	5.61	R1–R8/C134–C139:	74.3

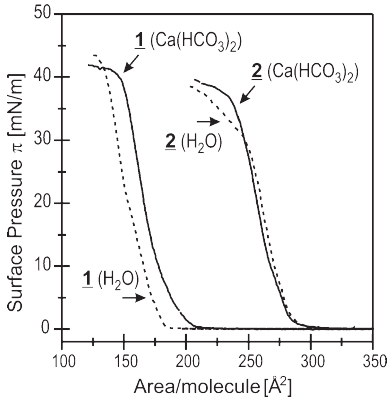

Fig. 5 π–A isotherms of monolayers of **1** and **2** at 22 °C on H_2O (dashed lines), and aqueous $CaCl_2/NaHCO_3$ (c = 9/18 mM, solid lines).

on an aqueous subphase containing $CaCl_2/NaHCO_3$ (c = 9/18 mM).

On both subphases, relatively stable monolayers of **1** form which collapse upon compression at a surface pressure of ~40 mN m^{-1} (pure water *or* Ca containing aqueous subphase). The featureless isotherms suggest fluid properties of the condensed monolayer phase. On pure water the onset of pressure increase is at ~190 $Å^2$ $molecule^{-1}$ whereas the surface pressure of the Ca containing solution starts to rise at a significantly higher value (~210 $Å^2$ $molecule^{-1}$). We assume that this behaviour is due to electrostatic or coordinative interactions of Ca ions which cause the carboxylic acid residues of **1** to become deprotonated. Expansion effects of monolayers spread on metal ion-containing subphases, similar to those observed here, have been reported for several systems.[15]

The area per molecule of **1** in the monolayers is estimated from extrapolating the Langmuir isotherms toward zero pressure. The determined area values are listed in Table 1. Monolayer data are in excellent agreement with the surface area per molecule as determined from crystal structure analysis. The monolayer data indicate that the packing densities of ligand **1** in the monolayer and in the crystal lattice are similar. The two-dimensional packing arrangement of **1** in the monolayer is presumably determined by the (highly solvated) polar carboxylate residues and not by the alkyl chains (for the latter case, a much more complicated monolayer phase behavior should be observed).

BAM images of monolayers of **1** on subphases containing pure water show that already at zero pressure the liquid-condensed monolayer phase forms, which is in agreement with previous reports.[16] The monolayers appear homogeneous within the spatial resolution limit of the BAM. When the collapse pressure is reached and upon further compression, the BAM micrographs display white spots indicating that double-layers are formed (images not shown). $CaCO_3$ crystallization experiments show that the phase region which appears homogeneously in the BAM (corresponding to a pressure range of π ~ 20–25 mN m^{-1}) provides optimal conditions for the growth of *aragonite* crystals (see below).

The calix[8]arene **2** also forms stable monolayers on pure water or Ca-containing aqueous subphases. On both subphases the pressure increase starts at the same molecular area of ~310 $Å^2$ $molecule^{-1}$.[17] The isotherms are almost identical indicating similar phase behaviour. In both cases the mean area per molecule in the monolayer amounts to ~280 $Å^2$ $molecule^{-1}$, which is approximately twice the area that we have previously determined for the corresponding tetracarboxy-calix[4]arenes (**4**).[9] Here, the adsorption layer of Ca ions underneath the monolayer of **2** does not lead to a detectable expansion as opposed to the compression behaviour we have perceived for charged monolayers of calix[4]arenes and resorc[4]arenes.

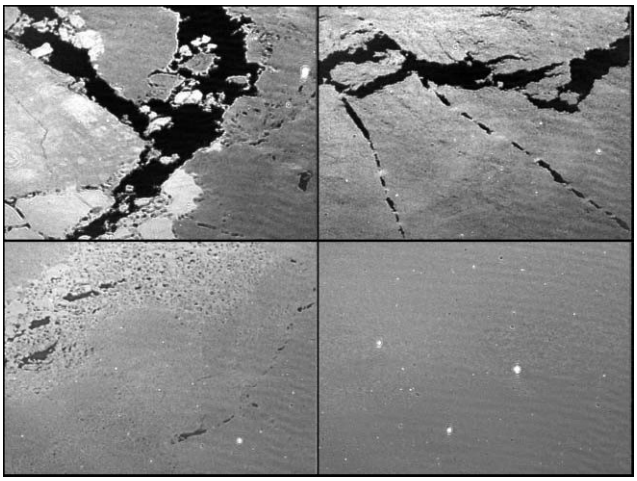

Fig. 6 BAM micrographs of monolayers of **2** at 24 °C on 10 mM $CaCl_2$. Monolayer domains appear as light regions. All micrographs were recorded at identical surface pressure (π = 0.1 mN m^{-1}) within a period of 5 minutes. The micrographs show representative morphologies at different sections of the monolayer. Areas of different brightness indicate that liquid-expanded phases coexist with liquid-compressed domains. Imaged area size: 430 × 320 μm^2.

Investigations on monolayers of **2** on aqueous subphases containing Cd ions have shown the same effect[18] which has been ascribed to the conformational flexibility of the molecules. Another explanation might be that the packing of **2** in the monolayer is dictated by the bulky 1,1,3,3-tetramethylbutyl substituents attached to the upper rim of the calix[8]arene macrocycle.

BAM investigations corroborate that there is in fact no difference in monolayer phase behaviour of **2** if spread on different subphases (H_2O or 10 mM $CaCl_2$). Fig. 6 shows a typical sequence of BAM images at near-zero surface pressure. The BAM images demonstrate that already at zero pressure the liquid-expanded (LE) phase coexists with liquid-condensed (LC) domains (areas of different brightness). Since the intensity of the polarized beam reflected from the monolayer shows a delicate dependence on film thickness the observed brightness alterations in the BAM micrographs might be due to different inclination angles of the molecules in the monolayer of **2**. Upon further compression (π > 0.1 mN m^{-1}) the monolayer appears homogeneous until the collapse pressure is reached when bright dots indicate formation of a multilayer (not shown). The pressure region where the monolayer of **2** displays LE and LC domains (π = 0.0–0.2 mN m^{-1}, ~330–350 $Å^2$ $molecule^{-1}$) leads to the growth of uniformly oriented *calcite* single crystals (see below). The coexistence of LC domains and a LE phase at near-zero surface pressure might be the reason for a reduced nucleation density of calcite single crystals as compared to the corresponding tetracarboxy-calix[4]arene (**4**) the monolayer of which appears more homogeneous in the same pressure range.

$CaCO_3$ Crystallization underneath monolayers of 1 and 2

Crystallization of $CaCO_3$ underneath a compressed monolayer of **1** leads to formation of aragonite crystals in the medium surface pressure range (π = 20–25 mN m^{-1}). When the compression is reduced the fraction of calcite rhombohedra and vaterite florets increases which constitute the predominant crystal species at low surface pressure (π = 0–2 mN m^{-1}). The majority of calcite rhombohedra are wedge-shaped crystals with an elevated central region and {104} cleavage planes.[19] Morphologically similar crystals were reported previously.[20] Based on electron diffraction from crystals at an early growth stage the authors have concluded that this particular morphology is due to nucleation originating from the $\{1\bar{1}0\}$ crystal face.[21]

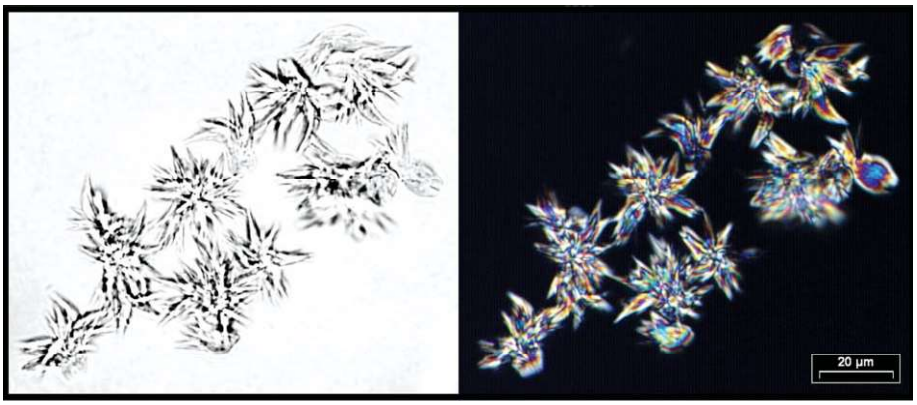

Fig. 7 Left: Brightfield optical micrograph of crystals grown under a monolayer of **1** after 3 h ($\pi = 20$ mN m^{-1}, $CaCl_2/NaHCO_3$ ($c = 9/18$ mM)). Right: Same crystal specimen observed in plane polarized light. (The viewing direction is parallel to the monolayer surface normal, crystals are observed from below the aqueous subphase).

Crystal growth was observed *in situ* by optical microscopy (Fig. 7). Aragonite crystals which grow underneath monolayers of **1** at high surface pressure display the typical acicular morphology of aragonite needles. In addition, varying amounts of vaterite florets form occasionally which are sometimes hardly distinguishable from the aragonite aggregates based on optical micrographs. A closer examination of crystal morphologies by scanning electron micrographs reveals that the aragonite crystal aggregates develop from a central pseudo-hexagonal basal plate which attaches to the monolayer at a central elevation (Fig. 8). This growth process is followed by secondary nucleation of a bunch of needle-type crystallites originating from the central primary crystal nucleus which leads to an over-all "comet-like" appearance of crystal habit.

Owing to the small amounts of crystalline material available through monolayer-directed crystallization and due to the fact that the crystal aggregates which are withdrawn from the water surface lose their original orientations, we were unable to obtain an X-ray diffraction pattern of sufficient quality employing a standard X-ray powder diffractometer. Instead we inserted a collection of representative crystals into mark capillaries and the X-ray diffraction pattern from the sample was collected by a rotation image using the 1 K CCD area detector of a four circle automated X-ray diffractometer.

Fig. 9 shows a typical X-ray diffraction image of $CaCO_3$ crystals grown underneath compressed monolayers of **1**. For a quantitative mineral phase analysis the angular diffraction limits were calibrated against a polycrystalline Si reference sample and the intensities of the Debye rings were extracted from the scattering image by integration and normalization of radial brightness profiles. The relative quantities of $CaCO_3$ polymorphs in the sample were determined by fitting a superposition of theoretical diffraction patterns of calcite, aragonite and vaterite to the experimentally observed pattern. The background originating from diffuse X-ray scattering of the glass capillary and amorphous components of the sample was taken into account by adding intensity values of a 7th order polynom function to the theoretical curve. Fig. 10a shows the experimental diffraction pattern together with the sum function of the simulated diffraction pattern and the background. The calculated sample composition indicates that aragonite constitutes the major mineral phase (approx. 80($\pm$10)%) followed by calcite (approx. 19($\pm$10)%). The

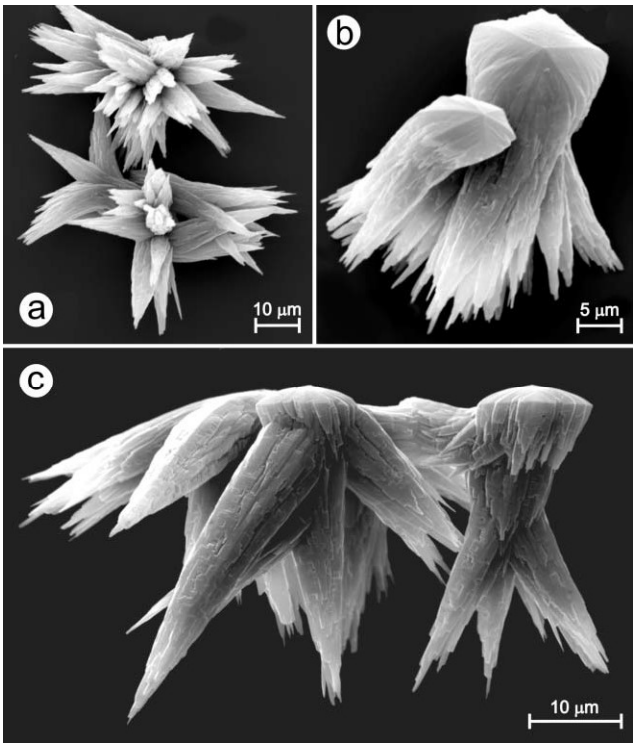

Fig. 8 Scanning electron micrographs (crystals collected after 6 h) of crystals grown under a monolayer of **1** ($\pi = 20$ mN m^{-1}, $CaCl_2/NaHCO_3$ ($c = 9/18$ mM). Approximate viewing directions are (a) from below, (b) from the top, and (c) from the side of the monolayer.

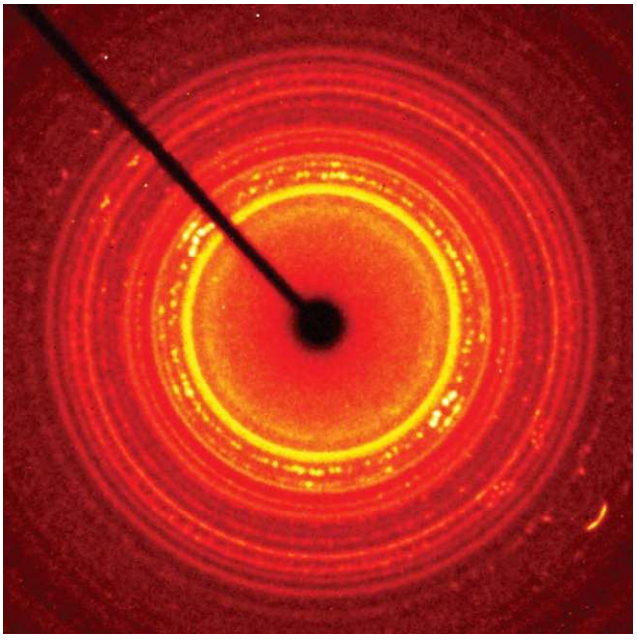

Fig. 9 XRD image from $CaCO_3$ crystals grown underneath a monolayer of **1**. (Rotation image, Mo-Kα X-ray beam).

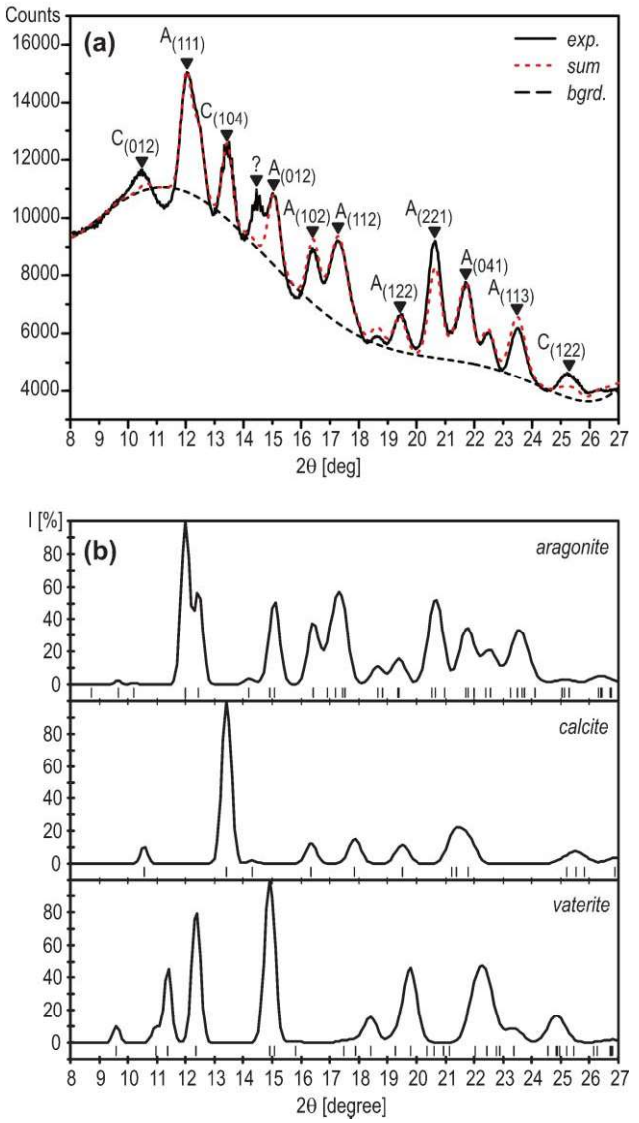

Fig. 10 (a) XRD pattern (solid line) from $CaCO_3$ crystals grown underneath a monolayer of **1** extracted from the rotation image. The simulated XRD pattern (red small dashes) of a mixture of aragonite/calcite/vaterite (81/18/1 vol%) and the calculated background (dashes). Crystallographic indices are presented in three-index (*hkl*) notation, based on the hexagonal setting of the calcite unit cell ($R\bar{3}c$, a = 4.96 Å, c = 17.002 Å) and the conventional setting of the orthorhombic unit cell of aragonite (*Pmcn*, a = 4.96 Å, b = 7.97 Å, c = 5.74 Å). (b) Simulated XRD pattern of different $CaCO_3$ polymorphs assuming a random orientation of crystal specimen. (Simulation parameters: λ = 0.71073 nm, Debye–Scherrer geometry, Gaussian peak profiles with empirically determined full width at half maximum values (FWHM = $f(u,v,w)$).

vaterite content of the sample is vanishing small ($<1\%$) which is somewhat surprising since the characteristic vaterite florets were ubiquitous in all samples. However, owing to the inherent broadness of the experimental diffraction peaks (Fig. 9) the accuracy of the phase analysis is somewhat limited and the exact composition values are slightly dependent on the refinement model.

Based on the results of quantitative phase analysis we therefore assume that the acicular crystal aggregates are composed of aragonite crystals. However, the observation of calcite diffraction peaks led us to explore the abundance of this $CaCO_3$ polymorph in more detail. From optical micrographs of $CaCO_3$ crystals grown underneath a compressed monolayer of **1** it becomes readily apparent that a small fraction of crystals consist of (non-truncated) calcite rhombohedra which spontaneously crystallize at the air–water interface regardless of the surface pressure employed. However, as a second option we considered the possibility that the primary nucleus of the acicular crystal aggregates might consist of calcite instead of aragonite. In order to obtain spatially resolved information of the mineral phase composition we employed fluorescence microscopy. The luminescence of $CaCO_3$ minerals is a well-documented feature which occurs commonly in $CaCO_3$ samples of geological and/or biological origin.[22] The weak luminescence is due to trace impurities of metal cations that replace Ca ions in the crystal lattice. Especially the presence of Mn^{2+} ions leads to intense luminescence of $CaCO_3$ crystals under various activation conditions (cathodoluminescence,[23] thermoluminescence[24]). Preliminary investigations have shown us that differentiation of $CaCO_3$ polymorphs should be feasible based on the characteristic luminescence of Mn^{2+} ions with the particular crystal fields of the host lattices leading to different wavelengths and decay times of the stimulated emission of photons. While a detailed analysis of the underlying physical principles is clearly beyond this work we note the experimental observation that morphologically distinct $CaCO_3$ crystals show clearly distinguishable emission colors if the sample is irradiated with intense UV light.

Fig. 11 shows the luminescence micrographs of representative crystal specimen grown underneath compressed monolayers of **1**. It is clearly seen that luminescence of the acicular crystal aggregates leads to a blue glow whereas the luminescence of the vaterite florets and rhombohedral calcite crystals (not shown) shows a significantly red-shifted (red–orange) glow. Furthermore, the luminescence of the acicular crystal aggregates appears homogeneous and we could not detect any regions showing different emission properties. Based on this experiment we conclude that the acicular crystal aggregates are uniformly composed of aragonite.

In contrast to **1**, monolayers of **2** lead to formation of uniformly oriented calcite single crystals at near-zero surface pressure (π = 0.0–0.2 mN m^{-1}). At a higher surface pressure (π = 0.5–25 mN m^{-1}) calcite rhombohedra form which lack any preferential orientation. The main orientation of calcite crystals grown underneath monolayers of **2** was determined by X-ray powder diffraction and geometrical analysis. A more detailed description of the procedure is given elsewhere.[9] The calcite single crystals obtained at low surface pressure underneath monolayers of **2** display the typical shape of truncated rhombohedra. The truncation occurs parallel to the {01.2} faces of the calcite crystal lattice. We have previously reported the identical growth behaviour for calcite crystals grown underneath monolayers of resorc[4]arenes and calix[4]arenes (Table 1). At high surface pressure non-truncated calcite {10.4} cleavage rhombohedra are observed. This indicates that at zero surface pressure the monolayer directs nucleation and growth of uniformly oriented calcite crystals while at higher surface pressure crystal growth becomes non-specific.[25]

Summary and conclusion

While in previous investigations we have employed monolayers of tetradentate amphiphilic macrocycles, we here report on the growth of $CaCO_3$ underneath monolayers of octadentate carboxylic acids. Compounds **1** and **2** were chosen for these investigations since they differ largely in the molecular surface area that each molecule can occupy in a monolayer. It is thus possible to adjust surface charge density underneath the monolayer by the appropriate selection of amphiphiles.

The molecular structures of all compounds investigated so far and their crystal packing arrangements differ significantly. Monolayers of amphiphilic calix[4]arene derivatives which possess hydrophobic substituents of varying steric demands have been employed[9] as well as amphiphilic resorc[4]arene derivatives[10] which are structurally complementary to the

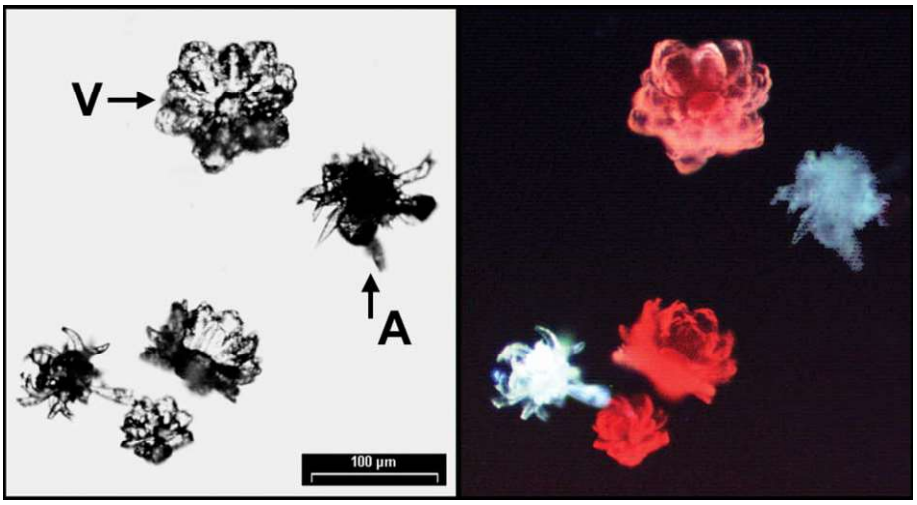

Fig. 11 Left: Brightfield optical micrograph of crystals grown under a monolayer of **1** after 14 h (π = 20 mN m^{-1}, $MnCl_2/CaCl_2/NaHCO_3$ (c = 0.04/9/18 mM)). Right: Same crystal specimen observed under UV light irradiation.

calix[4]arene ligands and show completely different Ca-coordination motifs.

Despite their structural and functional differences we observe the same orientation of calcite crystals which uniformly grow with their {01.2} crystal face attaching to the monolayers. In particular, the oriented growth of truncated calcite single crystals always and exclusively occurs at very low surface pressure, where the monolayers exist in a liquid-expanded state, an epitaxial correlation of the putative monolayer "lattice" and the {01.2} calcite crystal face can therefore be ruled out.

The templating role of monolayers has frequently (and perhaps without justification) been interpreted in terms of a geometrical and stereochemical complementarity between the arrangement of headgroups in the monolayer and the position of Ca ions in the crystal plane which attaches to the monolayer. Our investigations, however, clearly demonstrate that such delicate and complex interactions most likely vanish if structurally mobile template matrices such as monolayers are employed. Most probably non-specific electrostatic effects such as the average charge density or the mean dipole moment of the monolayer determine the orientation of crystals.[26]

In fact, for monolayers of **2** and many other (structurally different) amphiphiles the growth of (01.2) oriented calcite crystals occurs at a surface pressure where the average density of carboxylate residues at the air–water interface is about 2.00–2.44 COO^- nm^{-2} (Table 1).

It is therefore noteworthy that $CaCO_3$ crystallization underneath monolayers of **1** as reported in this work shows completely different characteristics, namely the formation of acicular aragonite crystal aggregates at high surface pressure and at an ionic composition of the aqueous subphase that would normally yield the thermodynamically more stable calcite. A similar behaviour has been reported earlier for a monolayer of 5-hexadecyloxyisophthalic acid.[27] The average charge density as derived from X-ray structure analysis of this compound amounts to 4.65 COO^- nm^{-2}.[28] Interestingly, crystallization of aragonite underneath monolayers of **1** occurs at a surface pressure where the charge density assumes a similar value (4.65–5.00 COO^- nm^{-2}, Table 1) which adds further support to our hypothesis that non-directional interfacial electrostatics is the dominant effect in template-directed crystal growth of $CaCO_3$ under Langmuir monolayers. Crystallization of aragonite from an aqueous subphase lacking soluble (organic) additives has been achieved quite a few times.[29] Experimental evidence as described here together with previous literature notes indicate that monolayer molecules possessing a high charge density are able to induce and stabilize metastable crystal phases at the air–water interface. The formation of aragonite and vaterite in this and related cases is obviously under kinetic control.[30] More recently, kinetic effects were discussed in this context on the basis of *in-situ* grazing incidence X-ray diffraction experiments.[31]

We are currently investigating $CaCO_3$ growth underneath monolayers of 5,11,17,23-tetra-*tert*-butyl-25,27-dicarbonylmethoxy-26,28-dihydroxycalix[4]arene where the reduced number of carboxylic acid residues per molecule (two instead of four or eight) leads to completely different calcium carbonate growth characteristics. Future investigations will focus on crystallization on $CaCO_3$ underneath mixed monolayers of macrocyclic oligoacids such as compound **1** or **4** and their corresponding oligoalcohols such as *rccc*-4,6,10,12,16,18,22,24-octa(2-hydroxyethoxy)-2,8,14,20-tetra(*n*-undecyl)resorc[4]arene or 5,11,17,23-tetrakis(1,1,3,3-tetramethylbutyl)-25,26,27,28-tetra(2-hydroxyethoxy)calix[4]arene which are strong $CaCO_3$ crystallization inhibitors.[32] By inserting a nucleation active oligocarboxylic acid into a matrix of molecules which inhibits crystal growth we hope to achieve nucleation by single molecules.

Experimental

Synthesis

All solvents used were in p.a. quality or purified by distillation. Melting points were determined on a Büchi B-540 apparatus and are uncorrected. NMR spectra were measured on a Bruker DRX 500 (^{1}H-NMR: 500.13 MHz; ^{13}C-NMR: 125.77 MHz) instrument using 7.24 ppm/77.0 ppm for $CHCl_3$. IR spectra were recorded on a Perkin-Elmer 841 infrared spectrophotometer. ESI mass spectra were recorded using an Esquire 3000 ion trap mass spectrometer (Bruker Daltonik GmbH, Bremen, Germany) equipped with a standard ESI source. Samples were introduced by direct infusion with a spring pump. Nitrogen served both as the nebulizer gas and the dry gas. Helium served as cooling gas for the ion trap. Elemental analysis was carried out with a Perkin-Elmer 240 elemental analyzer.

***rccc*-4,6,10,12,16,18,22,24-Octakis-*O*-(isopropoxy(oxo)ethyl)-2,8,14,20-tetra(*n*-undecyl)-resorc[4]arene.** To a suspension of *rccc*-2,8,14,20-tetra(*n*-undecyl)resorc[4]arene[33] (3.00 g, 2.71 mmol) and anhydrous potassium carbonate (7.50 g, 54.3 mmol) in dry acetonitrile (250 mL) was added isopropyl bromoacetate (12.3 g, 8.80 mL, 67.8 mmol) within 5 min. The mixture was heated under reflux for 16 h and concentrated *in vacuo*, followed by dilution in a mixture of diethyl ether and water to separate the organic layer. The water layer was extracted with diethyl ether (3×) and the

combined organic layers were washed with water, brine and dried over magnesium sulfate. The solvent was removed *in vacuo* and the crude product was recrystallized twice from acetonitrile. After drying *in vacuo* the product (2.67 g, 1.40 mmol, 52%) was obtained as colourless crystals, mp 61 °C. ^{1}H-NMR (500 MHz, $CDCl_3$): δ = 0.84 (t, ^3J = 7.0 Hz, 12 H, C*H*$_3$–CH$_2$), 1.20 (d, ^3J = 6.2 Hz, 24 H, C*H*$_3$–CH), 1.235 (d, ^3J = 6.3 Hz, 24 H, CH–C*H*$_3$), 1.15–1.35 (m, 72 H, CH$_2$), 1.82 (m, 8 H, CH–C*H*$_2$), 4.20 (d, ^2J = 16.1 Hz, 8 H, OC*H*$_2$–COO), 4.22 (d, ^2J = 16.1 Hz, 8 H, OC*H*$_2$–COO), 4.56 (t, ^3J = 7.4 Hz, 4 H, Ar–C*H*–Ar), 5.05 (qq, ^3J = 6.3 Hz, ^3J = 6.3 Hz, 8 H, CH$_3$–C*H*–CH$_3$), 6.186 (s, 4 H, Ar–H), 6.57 (s, 4 H, Ar–H); MS (ESI) *m*/*z* 1928.5 ((M + Na)$^+$, 100); Elemental analysis calc. for $C_{112}H_{176}O_{24}$: C 70.56; H 9.30; found: C 70.57; H 9.27%.

***rccc*-4,6,10,12,16,18,22,24-Octakis-*O*-(carboxymethyl)-2,8,14, 20-tetra(*n*-undecyl)-resorc[4]arene (1).** The product was prepared according to a slightly modified literature procedure.[34] *rccc*-4,6,10,12,16,18,22,24-Octakis-*O*-(isopropoxy(oxo)ethyl)-2,8,14,20-tetra(*n*-undecyl)-resorc[4]arene (1.00 g, 524 mmol) was dissolved in ethanol (100 mL) and lime potash (50 mL, 20%) and potassium hydroxide (10.0 g, 179 mmol) was added under argon. The mixture was heated under reflux for 10 d and concentrated under reduced pressure. The alkaline solution was rinsed with diluted hydrochloric acid, and the suspension was extracted with ethyl acetate (4 × 500 mL). The combined organic layers were washed with diluted hydrochloric acid and dried over sodium sulfate. The solvent was removed *in vacuo* and the crude product was recrystallized from methanol/water. After drying *in vacuo* the product (798 mg, 508 μmol, 97%) was obtained as white solid, mp 220 °C. Colourless crystals of **1** were obtained by recrystallization from an acetic acid/H_2O solvent mixture (95/5 vol%). ^{1}H-NMR (500 MHz, $CDCl_3$): δ = 0.92 (t, ^3J = 7.1 Hz, 12 H, C*H*$_3$–CH$_2$), 1.25–1–45 (m, 72 H, CH$_2$), 1.89 (m, 8 H, CH–C*H*$_2$), 4.30 (d, ^2J = 16.4 Hz, 8 H, OC*H*$_2$–COOH), 4.42 (d, ^2J = 16.4 Hz, 8 H, OC*H*$_2$–COOH), 4.71 (t, ^3J = 7.3 Hz, 4 H, Ar–C*H*–Ar), 6.438 (s, 4 H, Ar–H), 6.706 (s, 4 H, Ar–H); MS (ESI) *m*/*z* 1586.9 ((M + NH$_4$)$^+$, 100); Elemental analysis calc. for $C_{88}H_{128}O_{24}\cdot CH_3COOH\cdot(H_2O)_2$: C 64.88; H 8.23; found: C 65.09; H 8.22%.

5,11,17,23,29,35,41,47-Octakis(1,1,3,3-tetramethylbutyl)-49,50,51,52,53,54,55,56-octa(ethoxycarbonylmethoxy)calix[8]-arene (2b). The product was synthesized as described for the *tert*-butyl-derivative requiring additional recrystallization steps to give a crystalline product,[35] mp 120 °C (ethanol). ^{1}H NMR (500 MHz, $CDCl_3$) δ = 6.88 (s, 16 H, Ar*H*), 4.02–4.17 (m, 32 H, OC*H*$_2$COO, Ar–C*H*$_2$–Ar), 1.56 (s, 16 H, CC*H*$_2$C), 1.08 (s, 48 H, C*H*$_3$), 0.68 (s, 72 H, C*H*$_3$); IR (KBr) 1757 cm^{-1}; MS (ESI) *m*/*z* 2457.4 ((M + K)$^+$, 100); Elemental analysis calc. for $C_{152}H_{224}O_{24}$: C 74.96; H 9.27; found: C 74.90; H 9.30%.

5,11,17,23,29,35,41,47-Octakis(1,1,3,3-tetramethylbutyl)-49, 50,51,52,53,54,55,56-octa(carboxymethoxy)calix[8]arene (2). The product was prepared according to a slightly modified literature procedure.[36] To a solution of 5,11,17,23,29,35,41,47-octakis(1,1,3,3-tetramethylbutyl)-49,50,51,52,53,54,55,56-octa-(ethoxycarbonylmethoxy)calix[8]arene (0.70 g, 0.5 mmol) in tetrahydrofuran (30 mL) was added an aqueous solution of tetramethylammonium hydroxide (25%, 12 mL, 33 mmol). The suspension was heated under reflux. After 24 h the suspension was acidified with hydrochloric acid and chloroform was added. The organic layer was concentrated *in vacuo*, redissolved in chloroform, acidified with hydrochloric acid and washed with brine. After drying the organic layer over sodium sulfate and removing the solvent *in vacuo*, the crude product was suspended in acetonitrile to give the final product as white solid, mp > 265 °C (decomp.). ^{1}H-NMR (500 MHz, $CDCl_3$, 50 °C): δ = 6.95 (s, 16 H, Ar*H*), 4.19 (s, 16 H, OC*H*$_2$COO), 3.96 (s, 16 H, Ar–C*H*$_2$–Ar), 1.60 (s, 16 H, CC*H*$_2$C), 1.19 (s, 48 H, C*H*$_3$), 0.69 (s, 72 H, C*H*$_3$); MS (ESI) *m*/*z* 2247.3 ((M + K)$^+$, 100); Elemental analysis calc. for $C_{136}H_{192}O_{24}$: C 73.88; H 8.75; found: C 73.60; H 8.96%.

X-Ray structure analysis

Details of structure refinement and X-ray crystallographic data are provided as ESI with key data summarised in Table 3.

CCDC reference numbers 232971 (compound **1**) and 232972 (compound **2b**).

See http://www.rsc.org/suppdata/jm/b4/b403132f/ for crystallographic data in CIF or other electronic format.

Monolayer investigations

Monolayer experiments were performed with a double-barrier NIMA trough using a compression speed of 15 cm^2 min^{-1}. The surface pressure of the monolayers was measured using a Wilhelmy plate. Langmuir monolayers were formed on an aqueous subphase by spreading compound **1** from a trichloromethane/tetrahydrofuran (4 : 1) solution (30 μL, 0.1 mg mL^{-1}) and **2** from a 0.23 mM trichloromethane/methanol (9 : 1) solution (10 μL, 0.5 mg mL^{-1}). Compression was started after 10 min. Brewster angle microscopy were performed with a NIMA Langmuir trough (NIMA 601BAM) using a BAM-2 (NFT, Göttingen).

$CaCO_3$ crystal growth experiments

Solutions of calcium bicarbonate were prepared by bubbling carbon dioxide gas through a stirred aqueous (double deionized water, resistance 18.2 MΩ cm) solution of $CaCl_2$/$NaHCO_3$ (c = 9/18 mM) for a period of 2 h. Compressed films were formed by spreading the solutions of surfactants in order to generate a liquid-expanded or liquid-condensed film at the air–water interface. Crystals were studied after several times either *in situ* by optical microscopy (PZO Biolar upright microscope) or on cover slips laid on the film (Olympus IX70). The cover slips were also mounted on scanning electron microscope (SEM) specimen tubs. A Phillips XL30 ESEM operating at 30 keV was used. The calcite crystals were sputtered with Au prior to examination.

X-Ray diffraction and $CaCO_3$ mineral phase analysis

$CaCO_3$ crystals grown underneath monolayers of **2** were obtained by collecting crystals on glass cover slips laid on the film and removed horizontally. A Philips PW 1050/70 X-ray powder diffractometer was employed (2θ scans, Bragg–Brentano para-focussing geometry) using Cu-Kα radiation (λ = 1.54 Å).

$CaCO_3$ crystals grown underneath monolayers of **1** were obtained similarly. Due to the irregular crystal habits and the occurrence of three different $CaCO_3$ polymorphs the intensity of the experimental diffraction pattern was insufficient. Therefore, crystals were filled in a mark capillary with 0.2 mm diameter. A Bruker Nonius 1 K CCD diffractometer was employed using Mo-Kα radiation (λ = 0.71073 Å). The reflections were measured in rotation at a detector distance of 5 cm (2θ < 27°). The intensity was integrated using the program GADDS V3.317. Quantitative mineral phase analysis was performed with the software PowderCell V2.3.[37]

Luminescence experiments

To a solution of $CaCl_2$/$NaHCO_3$ (c = 9/18 mM) was added $MnCl_2$ (c = 0.04 mM). Compressed monolayers were formed as described above. After 14 h the crystals were transferred onto cover slips and sorted by hand. Selected specimens were examined by fluorescence microscopy using an inverted stage microscope (Olympus IX 70). The sample was illuminated with a 100 W high-pressure mercury lamp using a U-MWU2 mirror unit (wideband UV excitation at 330–385 nm, 420 nm emission

Table 3 X-Ray crystallographic data for compounds **1** and **2b**

Compound	**1**	**2b**
Formula	$C_{88}H_{128}O_{24}\cdot CH_3COOH\cdot(H_2O)_2$	$C_{152}H_{224}O_{24}\cdot C_2H_5OH\cdot H_2O$
M_r/g mol^{-1}	1665.99	2499.40
T/K	188(2)	183(2)
λ/Å	0.71073	0.71073
Crystal system	Triclinic	Monoclinic
Space group	$P\bar{1}$	$C2/c$
a/Å	9.9409(7)	34.9691(15)
b/Å	17.2656(11)	18.4700(8)
c/Å	27.3161(18)	49.942(2)
α/°	71.909(1)	90
β/°	83.817(1)	108.521(1)
γ/°	84.922(1)	90
V/Å^3	4423.2(5)	30586(2)
Z	2	8
ρ_{calc}/g m^{-3}	1.251	1.086
μ(Mo-Kα)/mm^{-1}	0.092	0.072
F(000)	1800	10912
Crystal size/mm	0.80 × 0.15 × 0.06	0.44 × 0.36 × 0.24
θ range/°	1.24–25.02	1.39–25.02
Index ranges	$-11 \leqslant h \leqslant 11$, $-20 \leqslant k \leqslant 20$, $-32 \leqslant l \leqslant 32$	$-38 \leqslant h \leqslant 41$, $-21 \leqslant k \leqslant 21$, $-59 \leqslant l \leqslant 52$
Reflections collected	39701	77537
R(int)	0.0511	0.0448
Independent reflections	15548	26912
Data/restraints/parameters	15548/6/1093	26912/0/1665
GoF	1.326	1.034
R values $[I > 2\sigma(I)]^a$	$R_1 = 0.1129$, $wR_2 = 0.3395$	$R_1 = 0.0834$, $wR_2 = 0.2259$
R values (all data)^a	$R_1 = 0.1704$, $wR_2 = 0.3800$	$R_1 = 0.1249$, $wR_2 = 0.2601$
Weighting scheme, w^{-1b}	$[s^2(F_o^2) + (0.2000\cdot P)^2]$	$[s^2(F_o^2) + (0.1316P)^2 + 74.16P]$
Largest diff. peak/hole/e Å^{-3}	1.335/−0.568	1.256/−1.173

^{a} $R_1 = \Sigma||F_o| - |F_c||/\Sigma|F_o|$; $wR_2 = [\Sigma w(F_o^2 - F_c^2)^2/\Sigma w(F_o^2)^2]^{1/2}$. ^{b} $P = (F_o^2 + 2F_c^2)/3$.

filter, 400 nm dichromatic mirror). Luminescence optical micrographs were recorded with a Hitachi HV-C20A 3-CCD RGB camera at a resolution of 3 × 768 × 576 pixels.

Acknowledgements

D. V. thanks the DFG for a Habilitanden fellowship. M. F. thanks the Graduiertenförderung Nordrhein-Westfalen for a graduate fellowship. We thank L. Chi and M. Gleiche of the faculty of interface physics (University of Münster) for providing access to BAM instruments. We thank M. Schmidtmann (University of Bielefeld, AC1) for XRD measurements. Donation of the starting material *p*-1,1,3,3-tetramethylbutylphenol by CONDEA Chemie GmbH (Marl, Germany) is gratefully acknowledged. This work was financially supported by the Deutsche Forschungsgemeinschaft (DFG Schwerpunktprogramm 1117, "Prinzipien der Biomineralisation"; DFG grant Vo829/2-1) and by the Fonds der Chemischen Industrie.

References and notes

1 (*a*) H. A. Lowenstam and S. Weiner, *On Biomineralization*, Oxford University Press, Oxford, 1989; (*b*) S. Mann, *Biomineralization. Principles and Concepts in Bioinorganic Materials Chemistry*, Oxford University Press, Oxford, 2001; (*c*) L. Addadi and S. Weiner, *Angew. Chem., Int. Ed. Engl.*, 1992, **31**, 153–169.

2 (*a*) S. Mann, *Biomimetic Materials Chemistry*, VCH, Weinheim, 1996; (*b*) S. Mann, D. D. Archibald, J. M. Didymus, T. Douglas, B. R. Heywood, F. C. Meldrum and N. J. Reeves, *Science*, 1993, **261**, 1286–1292.

3 (*a*) A. M. Belcher, X. H. Wu, R. J. Christensen, P. K. Hansma, G. D. Stucky and D. E. Morse, *Nature*, 1996, **381**, 56–58; (*b*) Y. Levi, S. Albeck, A. Brack, S. Weiner and L. Addadi, *Chem. Eur. J.*, 1998, **4**, 389–396.

4 (*a*) S. Mann, B. R. Heywood, S. Rajam and J. D. Birchall, *Nature*, 1988, **334**, 692–695; (*b*) S. Champ, J. A. Dickinson, P. S. Fallon, B. R. Heywood and M. Mascal, *Angew. Chem., Int. Ed.*, 2000, **39**, 2716–2719; (*c*) P. J. J. A. Buijnsters, J. J. J. M. Donners, S. J. Hill, B. R. Heywood, R. J. M. Nolte, B. Zwanenburg and N. A. J. M. Sommerdijk, *Langmuir*, 2001, **17**, 3623–3628.

5 (*a*) J. Aizenberg, A. J. Black and G. M. Whitesides, *Nature*, 1999, **398**, 495–498; (*b*) J. Küther, G. Nelles, R. Seshadri, M. Schaub, H. J. Butt and W. Tremel, *Chem. Eur. J.*, 1998, **4**, 1834–1842; (*c*) D. D. Archibald, S. B. Qadri and B. P. Gaber, *Langmuir*, 1996, **12**, 538–546.

6 (*a*) A. Berman, D. J. Ahn, A. Lio, M. Salmeron, A. Reichert and D. Charych, *Science*, 1995, **269**, 515–518; (*b*) H. Cölfen and M. Antonietti, *Langmuir*, 1998, **14**, 582–589; (*c*) A. Becker, W. Becker, J. C. Marxen and M. Epple, *Z. Anorg. Allg. Chem.*, 2003, **626**, 2305–2311.

7 (*a*) L. Addadi, J. Moradian, E. Shay, N. G. Maroudas and S. Weiner, *Proc. Natl. Acad. Sci. U. S. A.*, 1987, **84**, 2732–2736; (*b*) S. R. Letellier, M. J. Lochhead, A. A. Campbell and V. Vogel, *Biochim. Biophys. Acta*, 1998, **1380**, 31–45.

8 (*a*) L. Addadi and S. Weiner, in *Biomineralization*, S. Mann, ed., VCH, Weinheim, 1989, pp. 133–156; (*b*) J. Aizenberg, A. J. Black and G. M. Whitesides, *J. Am. Chem. Soc.*, 1999, **121**, 4500–4509.

9 (*a*) D. Volkmer, M. Fricke, D. Vollhardt and S. Siegel, *J. Chem. Soc., Dalton Trans.*, 2002, 4547–4554; (*b*) D. Volkmer and M. Fricke, *Z. Anorg. Allg. Chem.*, 2003, **629**, 2381–2390.

10 D. Volkmer, M. Fricke, C. Agena and J. Mattay, *CrystEngComm.*, 2002, **4**, 288–295.

11 Average values are calculated from crystallographic independent parameters of two molecules in the asymmetric unit of compound **3** (CCDC reference number 183961).

12 C. D. Gutsche, *Calixarenes, Monographs in Supramolecular Chemistry*, J. F. Stoddart,ed., The Royal Society of Chemistry, Cambridge, 1989, pp. 149–185.

13 R. Ungaro, A. Pochini, G. D. Andreetti and F. Ugozzoli, *J. Inclusion Phenom. Macro. Chem.*, 1985, **3**, 409–420 . CCDC structure code DIZVEN.

14 The compound 5,11,17,23,29,35,41,47-octakis(1,1,3,3-tetramethylbutyl)-49,50,51,52,53,54,55,56-octakis(2-methoxyethoxy)calix(8)arene (CCDC structure code DIZVEN) forms close packed layers in the $\{\bar{1}01\}$ crystal plane. The calculated surface area/molecule here amounts to 3.03 nm^2 which is roughly 7% less than the average surface area of **2b**.

15 (*a*) V. A. Arsentiev and J. Leja, in *Colloid and Interface Science*, M. Kerker, ed., **vol. 5**, Academic Press, New York, 1976, pp. 251–270; (*b*) G. T. Barnes, in *Colloid Science*, D. H. Everett, ed., **vol. 2**, Chemical Society, London, 1975, pp. 173–190.

16 Y. Matsuzawa, S. Takahiro and K. Ichimura, *J. Inclusion Phenom. Macro. Chem.*, 1999, **35**, 199–210.

17 T. Richardson, M. B. Greenwood, F. Davis and C. J. M. Stirling, *Langmuir*, 1995, **11**, 4623–4625.

18 A. V. Nabok, T. Richardson, F. Davis and C. J. M. Stirling, *Langmuir*, 1997, **13**, 3198–3201.
19 Crystallization of $CaCO_3$ underneath monolayers of stearic acid yield crystals displaying the same morphology: S. Mann, B. R. Heywood, S. Rajam and J. B. A. Walker, *J. Phys. D: Appl. Phys.*, 1991, **24**, 154–164.
20 S. Rajam, B. R. Heywood, J. B. A. Walker, S. Mann, R. J. Davey and J. D. Birchall, *J. Chem. Soc., Faraday Trans.*, 1991, **87**, 727–734.
21 Representative optical and scanning electron micrographs of $CaCO_3$ crystals grown underneath a monolayer of **1** at low surface pressure are provided as ESI. The micrographs show calcite crystals possessing different orientations. There is currently no experimental evidence for $CaCO_3$ nucleation originating from the $\{1\bar{1}0\}$ crystal faces.
22 (*a*) A. S. Marfunin, in *Spectroscopy, luminescence and radiation centers in minerals*, Springer-Verlag, Berlin, 1979, ch. 5, pp. 141–220; (*b*) M. R. Krbetschek, J. Götze, A. Dietrich and T. Trautmann, *Radiat. Meas.*, 1997, **27**, 695–748.
23 G. M. Walkden and J. R. Berry, *Nature*, 1984, **308**, 525–527.
24 T. Calderón, P. D. Townsend, P. Beneitez, J. Garcia-Guinea, A. Millán, H. M. Rendell, A. Tookey, M. Urbina and R. A. Wood, *Radiat. Meas.*, 1996, **26**, 719–731.
25 S. J. Cooper, R. B. Sessions and S. D. Lubetkin, *J. Am. Chem. Soc.*, 1998, **120**, 2090–2098.
26 (*a*) M. J. Lochhead, S. R. Letellier and V. Vogel, *J. Phys. Chem. B*, 1997, **101**, 10821–10827; (*b*) P. Calvert and S. Mann, *Nature*, 1997, **386**, 127–129.
27 A. L. Litvin, S. Valiyaveettil, D. L. Kaplan and S. Mann, *Adv. Mater.*, 1997, **9**, 124–127.
28 S. Valiyaveetil, V. Enkelmann and K. Müllen, *J. Chem. Soc, Chem. Commun.*, 1994, 2097–2098.
29 B. R. Heywood and S. Mann, *Chem. Mater.*, 1994, **6**, 311–318.
30 (*a*) G. Falini, S. Fermani, M. Gazzano and A. Ripamonti, *Chem. Eur. J.*, 1998, **4**, 1048–1052; (*b*) K. Naka, D.-K. Keum, Y. Tanaka and Y. Chujo, *Chem. Commun.*, 2000, 1537–1538.
31 E. DiMasi, M. J. Oltsza, V. M. Patel and L. Gower, *CrystEngComm*, 2003, **5**, 346–350.
32 D. Volkmer, M. Fricke, M. Gleiche and L. Chi, *Mater. Sci. Eng. C*, accepted.
33 The starting compound *rccc*-2,8,14,20-tetra(n-undecyl)resorc[4]-arene was prepared according to a slightly modified literature procedure: L. M. Tunstad, J. A. Tucker, E. Dalcanale, J. Weiser, J. A. Byrant, J. C. Sherman, R. C. Helgeson, C. B. Knobler and D. J. Cram, *J. Org. Chem.*, 1989, **54**, 1305–1312.
34 E. Kurita, N. Fukushima, M. Fujimaki, Y. Matsuzawa, K. Kudo and K. Ichimura, *J. Mater. Chem.*, 1998, **8**, 397–403.
35 F. Arnaud-Neu, E. M. Collins, M. Deasy, G. Ferguson, S. J. Harris, B. Kaitner, A. J. Lough, M. A. McKervey, E. Marques, B. L. Ruhl, M. M. J. Schwing-Weill and E. M. Seward, *J. Am. Chem. Soc.*, 1989, **111**, 8681–8691.
36 S.-K. Chang and I. Cho, *J. Chem. Soc., Perkin Trans. 1*, 1986, 211–214.
37 PowderCell 2.3 for Windows. Copyright W. Kraus, G. Nolze, Federal Institute for Materials Research and Testing (Berlin, Germany). The software can be downloaded free of charge from ftp://ftp.bam.de/Powder_Cell/ or from the current link *via* the CCP14 homepage http://www.ccp14.ac.uk/ccp/ccp14/ftp-mirror/powdcell/Powder_Cell/.